Available online at www.sciencedirect.com
ScienceDirect
Journal of Sound and Vibration 319 (2009) 1150–1174
JOURNAL OF SOUND AND VIBRATION
www.elsevier.com/locate/jsvi

Nonlinear dynamic modeling of surface defects in rolling element bearing systems

Ahmad Rafsanjani[a,*], Saeed Abbasion[a], Anoushiravan Farshidianfar[b], Hamid Moeenfard[c]

[a]*Department of Mechanical Engineering, Iran University of Science & Technology, Tehran, Iran*
[b]*Department of Mechanical Engineering, Ferdowsi University of Mashhad, Mashhad, Iran*
[c]*Department of Mechanical Engineering, Sharif University of Technology, Tehran, Iran*

Received 9 February 2008; received in revised form 25 June 2008; accepted 25 June 2008
Handling Editor: C.L. Morfey
Available online 6 August 2008

Abstract

In this paper an analytical model is proposed to study the nonlinear dynamic behavior of rolling element bearing systems including surface defects. Various surface defects due to local imperfections on raceways and rolling elements are introduced to the proposed model. The contact force of each rolling element described according to nonlinear Hertzian contact deformation and the effect of internal radial clearance has been taken into account. Mathematical expressions were derived for inner race, outer race and rolling element local defects. To overcome the strong nonlinearity of the governing equations of motion, a modified Newmark time integration technique was used to solve the equations of motion numerically. The results were obtained in the form of time series, frequency responses and phase trajectories. The validity of the proposed model verified by comparison of frequency components of the system response with those obtained from experiments. The classical Floquet theory has been applied to the proposed model to investigate the linear stability of the defective bearing rotor systems as the parameters of the system changes. The peak-to-peak frequency response of the system for each case is obtained and the basic routes to periodic, quasi-periodic and chaotic motions for different internal radial clearances are determined. The current study provides a powerful tool for design and health monitoring of machine systems.

1. Introduction

Rolling element bearings are one of the most widely used components in industrial applications. They have a great influence on the dynamic behavior of the rotating machines and act as a source of vibration and noise in these systems. There is a critical need to increase reliability and performance of rolling element bearings to prevent catastrophic failure of the machinery. Defects in bearings may arise during use or during the manufacturing process. Different methods are used for detection and diagnosis of bearing defects. Modeling

*Corresponding author.
E-mail addresses: rafsanjani@mecheng.iust.ac.ir, ahmad.rafsanjani@gmail.com (A. Rafsanjani).

0022-460X/$ - see front matter © 2008 Elsevier Ltd. All rights reserved.
doi:10.1016/j.jsv.2008.06.043

Nomenclature

c	damping coefficient, N s/m
D	pitch diameter, mm
d	ball diameter, mm
f_u	unbalance force, N
FFT	fast Fourier transform
$I_d(t)$	impulse due to inner race defect
K	constant for Hertzian contact elastic deformation, $N/m^{3/2}$
m	mass of inner race and the rotor, kg
$O_d(t)$	impulse due to outer race defect
R	pitch radius, mm
$R_d(t)$	impulse due to rolling element defect
R_i	inner race radius, mm
R_o	outer race radius, mm
r	ball radius, mm
t	time, s
W_x	horizontal component of radial force, N
W_y	vertical component of radial force, N
Z	number of balls
γ	internal radial clearance, μm
δ_j	deformation at the point of the contact of the jth rolling element, m
θ_j	angular position of the jth rolling element, rad
λ_j	loading zone parameter of the jth rolling element
ω	rotational speed of the shaft, rad/s
ω_b	ball spinning frequency, rad/s
ω_c	rotational speed of the cage, rad/s
ω_{bpi}	inner race defect frequency, rad/s
ω_{bpo}	outer race defect frequency, rad/s
ω_{vc}	varying compliance frequency, rad/s

and simulation methods provide an increasingly accurate approach for predicting the dynamic performance of systems that include ball bearings.

Radially loaded rolling element bearings generate vibration even if they are geometrically perfect. This is because of the use of a finite number of rolling elements to carry the load. The number of rolling elements and their position in the load zone change with bearing rotation, giving rise to a periodical variation of the total stiffness of the bearing assembly. This variation of stiffness generates vibrations commonly known as varying compliance vibrations [1]. However, the presence of a defect causes a significant increase in the vibration level. Bearing defects may be categorized as distributed or local. Distributed defects include surface roughness, waviness, misaligned races and off-size rolling elements [2]. They are usually caused by manufacturing error, improper installation or abrasive wear [3]. Local defects include cracks, pits and spalls on the rolling surfaces. The dominant mode of failure of rolling element bearings is spalling of the races or the rolling elements, caused when a fatigue crack begins below the surface of the metal and propagates towards the surface until a piece of metal breaks away to leave a small pit or spall [4]. Whenever, a local defect on an element interacts with its mating element, abrupt changes in the contact stresses at the interface result, which generates a pulse of very short duration. This pulse produces vibration and noise which can be monitored to detect the presence of a defect in the bearing.

A lot of research work has been published recently, on the detection and diagnosis of bearing defects [5–7]. Tandon and Choudhury [4] presented a complete review of vibration and acoustic measurement methods for the detection of defects in rolling element bearings. But just few works present mathematical models for simulation of local bearing defects and most of proposed models investigated the distributed defects particularly waviness of raceways [8–11].

The early works on mechanical modeling of localized bearing defects was performed by McFadden and Smith [12]. They proposed a vibration models for a single point defect on the inner race of a rolling element bearing under radial load. In this model the vibration is modeled as the product of a series of impulses at the rolling element passing frequency with the bearing load distribution and the amplitude of the transform function, convolved with the impulse response of the exponential decay function. They developed the single point defect model to describe the vibration produced by multiple point defects [13]. These models were experimentally verified by NASA researchers using nonlinear signal analysis techniques [14].

Tandon and Choudhury [15] proposed an analytical model for predicting the vibration frequencies of rolling bearings and the amplitudes of significant frequency components due to a localized defect on outer race, inner race or on one of the rolling elements under radial and axial loads. The defects described with finite width triangular, rectangular and half-sine pulses. The results showed that, when both radial and axial loading

exist the outer race defects generates vibration in the outer race defect frequency and its harmonics. For an inner race defects, in the absence of radial loading the vibration generated in the inner race defect frequency. But in the case of both radial and axial loading, the vibration generated in the inner race defect frequency and its sidebands at shaft frequency. They also reported that the vibration level is affected by the pulse shape.

Sopanen and Mikola [16,17] proposed a dynamic model for a deep-groove ball bearing including localized and distributed defects, effect of internal radial clearance and unbalance excitation of the system. The model considers the Hertzian contact deformation and elastohydrodynamic fluid film in rolling contacts. For the modeling purpose, the shape of the defect is described with the length and the height of the defect. The results of their simulation indicates that both inner ring and outer ring defects generates vibration at their nominal frequencies. They also found that the amplitude of the vibration for similar defects is higher for an outer race defect. This is because the outer ring defect is always in the load zone, and thus the pulse occurs every time a ball passes over the defect.

Cao and Xiao [18] presented a dynamic model for double-row spherical roller bearing and studied various surface defects, including localized and distributed ones in their model. The spherical roller bearing systems carries one more extra degree of freedom on the moving race so they formulated the roller inner/outer race contact angles as functions of the axial displacement of the moving race to reflect their dependence on the axial movement.

There is an urgent need to study the topological structure and stability of rotor bearing systems with ball bearings. There are a lot of parameters which can act as a source of nonlinearity in these systems such as radial internal clearance and also local surface defects. Recently, Tiwari et al. [19] and Harsha [20] investigated the stability of a rigid rotor supported by deep-groove ball bearings and described the unstable ranges for different radial clearances but the stability of a rolling bearing rotor system containing local surface defects has not been studied before.

In this paper a mathematical method was developed based on the two-degree-of-freedom nonlinear model proposed by Sunnersjo [1]. In this model, the rolling elements are modeled as nonlinear springs according to Hertzian contact theory and the effect of loading zone has been taken into account. Fulata et al. [21] analyzed the radial vibration of ball bearings derived from Sunnersjo's model. They reported the system may exhibit super-harmonic and sub-harmonic resonances, beat and chaotic vibrations. The surface defects including single point defects on raceways and rolling elements were introduced to this model with several mathematical expressions and the equations of motion were updated in each case. A modified Newmark time integration technique used to solve the equations of motion numerically [22]. The classical Floquet theory is applied to the proposed model to investigate the linear stability of the bearing system including local defects on raceways and rolling elements. Finally, the basic routes to chaos in rolling bearing systems are discussed in details.

2. Characteristic defect frequencies

There are some basic motions in rolling element bearings which demonstrate dynamics of the elements of rotating bearing and each has its specific frequency. These frequencies are illustrated in Fig. 1. They are cage

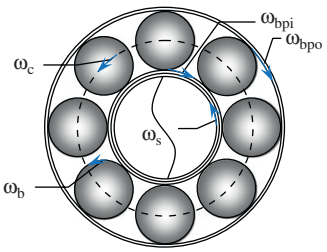

Fig. 1. Basic frequency in a bearing.

frequency (ω_c); ball passing inner race frequency (ω_{bpi}), ball passing outer race frequency (ω_{bpo}) and ball spin frequency (ω_b). These frequencies are known as defect frequencies of rolling element bearings (see Appendix A for more details). Any defect in bearing elements, results in an increase of vibration energy at defect frequencies or combination of them [23].

For normal speeds, these defect frequencies lie in the low-frequency range and are usually less than 500 Hz [4]. In practice, however, these frequencies may be slightly different from the calculated values as a consequence of slipping or skidding in the rolling element bearings [24].

3. Governing equations of motion

Consider the rolling element bearing is shown in Fig. 2. In this model which was developed by Sunnersjo [1], the inner race of the bearing is assumed to have two degrees of freedom. The contact forces are summed over each of the rolling elements to give overall forces on the shaft and bearing housing.

The overall contact deformation for the jth rolling element, δ_j, is given by

$$\delta_j = x\cos\theta_j + y\sin\theta_j - \gamma \tag{1}$$

where γ is the internal radial clearance. Neglecting the effect of rolling element inertia, the inner and outer race contact forces can be combined with an overall contact stiffness. The total restoring forces in x and y direction on the shaft and bearing housing is given by

$$f_x = K\sum_{j=1}^{Z}\lambda_j\delta_j^{1.5}\cos\theta_j$$

$$f_y = K\sum_{j=1}^{Z}\lambda_j\delta_j^{1.5}\sin\theta_j \tag{2}$$

where λ_j is the loading zone parameter for the jth rolling element:

$$\lambda_j = \begin{cases} 1 & \delta_j > 0 \\ 0 & \delta_j \leqslant 0 \end{cases} \tag{3}$$

In Eq. (2) Z is the number of rolling elements and K is the overall contact stiffness which is obtained from Hertzian deformation local to the contact zone. It depends on the geometry and material properties of the contacting surfaces [16]. θ_j is the angular position of the jth rolling element which is given by

$$\theta_j = \frac{2\pi(j-1)}{Z} + \omega_c t + \theta_0 \tag{4}$$

where ω_c is the cage frequency (see Appendix A) and θ_0 is the initial angular position of the first rolling element respect to x-axis.

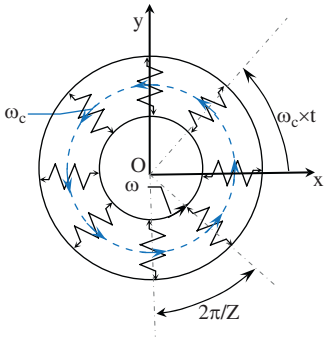

Fig. 2. Mass–spring model of rolling element bearing.

Now, the governing equations of motion can be obtained by applying the inertia, damping and restoring force to the inner race as following:

$$m\ddot{x} + c\dot{x} + f_x = W_x + f_u \cos \omega t \tag{5}$$

$$m\ddot{y} + c\dot{y} + f_y = W_y + f_u \sin \omega t \tag{6}$$

where m is the mass of inner race and the rotor supported by bearing and c is the equivalent viscous damping. W_x and W_y are the components of radial force acting on the rotor, f_u is the unbalance force which is taken for balanced rotor as zero and ω is the shaft frequency. The governing equations of motion (5) and (6) are two coupled strongly nonlinear second-order differential equations with parametric excitation.

4. Surface defect modeling

When a local defect such as pitting exists in one of the bearing components, a transient force occurs whenever another bearing component contacts the defective surface. A local fault produces an impulse having a repetition rate equal to the characteristic frequencies (Appendix A) of the bearing: ball passing frequency for the outer raceway, ball passing frequency for the inner raceway, and twice the ball spin frequency [25]. Although, this can cause quite complex reactions within the bearing, for the purpose of modeling, the reaction can be approximated by a short term impulses. The impulses are modeled using the following operator:

$$\Lambda_d(\theta) = \begin{cases} 1 & |\theta| \leqslant \theta_e \\ 0 & |\theta| > \theta_e \end{cases} \tag{7}$$

where θ_e is the half of the desired length of the defect in tangential direction. Separate equations are developed for each defect type. The amplitude of the impulse is affected by both the applied load and the angular velocity at the point of the contact; it can also be modulated due to relative motion of the load zone. The duration of contact between defect surface and rolling elements is too small, so the chosen impulse should last proportional to the ratio of length of the defected surface to the circumference of the race way in which the defect is located. The amplitude of the generated impulse is related to the loading ($\bar{L}$) and shaft speed and will be modulated due to relative motion of the balls towards the load zone.

4.1. Inner race defect

The vibration produced by inner race defect can be modeled as a series of impulses repeating with the frequency of inner race contact angle:

$$I_d(t) = \alpha_{id} A_{id}(h_{id}, \bar{L}, \omega) \sum_{j=1}^{Z} (1 + a_{id}(j)) \Lambda_d \left(\mathrm{mod}(\theta_{ij}, 2\pi) - \frac{2\pi}{Z}(j-1) - \varphi_{id} \right) \tag{8}$$

Also, the inner race contact angle θ_{ij}:

$$\theta_{ij} = \frac{2\pi}{Z}(j-1) + (\omega_c - \omega) \times t \tag{9}$$

α_{id} is the amplitude modulation due to relative motion of the load zone respect to inner race, $A_{id}(h_{id}, \bar{L}, \omega)$ is the mean impulse amplitude due to point defect with depth of h_{id}, $a_{id}(j)$ is the amplitude modulation due to the jth rolling element, φ_{id} is the initial angular offset of the defect to first rolling element.

In the above formulation, the effect of localized defects is modeled as an impulse sequence, which includes a summation over the number Z of all rolling and the impulse sequence is then further added to the radial displacement of each rolling element. It is notable that this summation over all rolling elements does not mean that each rolling element produces an impulse individually. This procedure just finds those rolling elements which pass the defective region on inner race surface by estimating the angular distance between defect

position and each rolling element. If this angular distance is less than defect size an impulse would be generated. Commonly, the defect size is small and just one rolling element at a certain time may pass the defective region, however the formulation was written for general case. So if the defect size is such large that at each time more than one rolling element contact it, the impulse amplitude would be modulated in the corresponding defect function (e.g. $I_d(t)$). Similarly, the above description may be explained for outer race and rolling element defects as formulated in the following sections.

4.2. Outer race defect

For the case of localized defect on the outer race the vibration model is similar to that produced by an inner race defect. So the vibration generated due to outer race defect can be expressed as

$$O_d(t) = \alpha_{od} A_{od}(h_{od}, \bar{L}, \omega) \sum_{j=1}^{Z} (1 + a_{od}(j)) \ \Lambda_d \left(\mathrm{mod}(\theta_{oj}, 2\pi) - \frac{2\pi}{Z}(j-1) - \varphi_{od} \right) \tag{10}$$

Since the outer ring is fixed the outer race contact angle is

$$\theta_{oj} = \frac{2\pi}{Z}(j-1) + \omega_c \times t \tag{11}$$

where α_{od} is the amplitude modulation due to relative motion of the load zone respect to inner race, $A_{od}(h_{od}, \bar{L}, \omega)$ is the mean impulse amplitude due to point defect with depth of h_{od}, $a_{od}(j)$ is the amplitude modulation due to the jth rolling element, φ_{od} is the initial angular offset of the defect to first rolling element.

4.3. Rolling element defect

When there is a defect on the ball surface, the defect impacts two times per revolution of the ball about its own axis, one for inner ring and another for outer ring. Assuming that the response is different for contact on the inner and outer race, but is the same each time the defect contacts a particular race, there will be a periodicity based on the rotation of the rolling element. The generated impulse due to ball defect during contact with inner and outer ring is expressed as below

$$R_{id}(t) = \alpha_{\mathrm{ir}d} A_{\mathrm{ir}d}(h_{bd}, \bar{L}, \omega) \Lambda_d(\mathrm{mod}(\theta_b, 2\pi) - \varphi_{bd}) \tag{12}$$

$$R_{od}(t) = \alpha_{\mathrm{or}d} A_{\mathrm{or}d}(h_{bd}, \bar{L}, \omega) \Lambda_d(\mathrm{mod}(\theta_b, 2\pi) - \pi - \varphi_{bd}) \tag{13}$$

And the total vibration generated due to rolling element defect can be expressed as

$$R_d(t) = R_{id}(t) + R_{od}(t) \tag{14}$$

where $\alpha_{\mathrm{ir}d}$ and $\alpha_{\mathrm{or}d}$ are the amplitude modulation due to relative motion of the load zone respect to cage for inner and outer race, respectively.

$A_{\mathrm{ir}d}(h_{bd}, \bar{L}, \omega)$ and $A_{\mathrm{or}d}(h_{bd}, \bar{L}, \omega)$ are the mean impulse amplitude for inner and outer race.

φ_{bd} is the initial angular offset of the defect to the inner race at $\theta_b = 0$.

5. Linear analysis of stability

The classical Floquet Theory is applied to the system of nonlinear differential Eqs. (5) and (6) to determine the linear stability of the bearing system. Consider

$$\dot{U}(t) = F(t, U(t), \sigma) \tag{15}$$

where σ is the bifurcation parameter and $U(t)$ and F defined as

$$U(t) = \begin{bmatrix} x & y & \dot{x} & \dot{y} \end{bmatrix}^{\mathrm{T}} \tag{16}$$

$$F = \begin{Bmatrix} \dot{x} \\ \dot{y} \\ -\frac{1}{m}\left(c\dot{x} + K\sum_{j=1}^{Z}\lambda_j\delta_j^{1.5}\cos\theta_j\right) \\ -\frac{1}{m}\left(c\dot{y} + K\sum_{j=1}^{Z}\lambda_j\delta_j^{1.5}\sin\theta_j\right) \end{Bmatrix} \tag{17}$$

The solution $\tilde{U}(t)$ of Eq. (15) is assumed to oscillate at the varying compliance frequency, so it has the period of $T = 1/\omega_{vc}$ where $\omega_{vc} = Z\Omega_{vc}$ is the varying compliance frequency, so that:

$$\tilde{U}(t) = \tilde{U}(t+T) \tag{18}$$

Substitution of the assumed solution (18) into Eq. (15) and introducing $u(t)$ as the perturbation of the periodic solution yields

$$\dot{\tilde{U}}(t) + \dot{u}(t) = F(t, \tilde{U}(t) + u(t), \alpha) \tag{19}$$

The Linearized perturbation equation can be determined by expanding F as the Taylor series expansion and considering just the linear terms:

$$\dot{u}(t) = \mathbf{A}(t)u(t) \tag{20}$$

where $\mathbf{A}(t) = \partial F/\partial\tilde{U}(t)$ which is a periodic function of period T. The elements of matrix $\mathbf{A}$ is given in Appendix C. By classical Floquet theory, any fundamental matrix $\mathbf{\Phi}$, which is defined as a non-singular matrix satisfying

$$\dot{\mathbf{\Phi}}(t) = \mathbf{A}(t)\mathbf{\Phi}(t) \tag{21}$$

Can be given as

$$\mathbf{\Phi}(t) = P(t)\exp(t\mathbf{R}) \tag{22}$$

$P(t)$ is a non-singular matrix of periodic functions with the same period T, and $\mathbf{R}$ is a constant matrix, whose eigenvalues are the characteristic exponents of dynamical system (20). If the fundamental matrix is normalized such that $\mathbf{\Phi}(t_0) = \mathbf{I}$, the monodromy matrix of the system (20) can be calculated as

$$\tilde{\mathbf{M}}_T = \exp(T\mathbf{R}) = \mathbf{\Phi}(t_0)\mathbf{\Phi}(t_0 + T) \tag{23}$$

The monodromy matrix $\tilde{\mathbf{M}}_T$ does not depend on the initial time t_0 [26]. The eigenvalues of monodromy matrix give the Floquet multiplier of the system which can be used to determine the linear stability of the periodic solutions as follows [27]:

(a) if all the multipliers are located within the unit circle, the system is stable,
(b) if one of the multipliers leaves the unit circle through -1, this indicates period multiplying bifurcations,
(c) if one of the multipliers leaves the unit circle through $+1$, this could indicate bifurcations, possibly including a saddle node,
(d) if a pair of complex conjugate multipliers is leaving the unit circle, a Hopf, or a secondary Hopf bifurcation could occur.

6. Numerical results

The governing equations of motion introduced in previous section are solved numerically using the modified Newmark time integration technique [22] and the response of the system was obtained. The overall contact deformation of the jth rolling element, δ_j, was updated to include the effect of each defect as $\delta_j = x\cos\theta_j + y\sin\theta_j - (\gamma + I(t))$. As introduced in previous sections $I(t)$ is the impulse function corresponding to each defect. The transient vibrations of the system were eliminated by introducing an appropriate damping to achieve the steady-state response of the system. For a given mass 0.6 kg and $W_y = 6$ N in the present study,

the damping coefficient was chosen to be 200 N m/s. As it was mentioned before when the bearing rotates the loaded zone will change as a function of time resulting in parametric excitations. In parametrically excited systems, it is always difficult to estimate the frequency content of the response in advance. This information is needed to determine the time step in the Newmark time integration method. Hence, in calculations the time step was chosen to be $\Delta t = 10^{-5}$. For fast convergence, the following initial conditions were applied to the system under investigation: initial displacements are ($x_0 = 1\,\mu m$, $y_0 = 1\,\mu m$) and the initial velocities set to be ($\dot{x}_0 = 0, \dot{y}_0 = 0$).

6.1. System under investigation

In the present study, the analysis applied to a 6205-2RSL JEM SKF deep-groove ball bearing. The bearing specifications including bearing geometry, defect frequencies and size of each defect are listed in Tables 1–3. This bearing used as motor shaft support at the drive end of a 2 hp, three-phase induction motor (left) (Reliance Electric 2HP IQPreAlert motor). There is also another bearing at the fan end of the motor which was not studied in this work. Single point faults were introduced to the test bearings using electro-discharge machining with fault diameters of 7 mil (1 mil = 0.001 in). Digital data were collected at 12,000 samples per second. The test stand is shown in Fig. 3. All data related to the bearing and the system under investigation belongs to Case Western Reverse Lab. and is with permission of Dr. Kenneth A. Loparo. More details about experimental setup are reported in Ref. [5].

To assure the validity of the proposed model, a number of simulated results compared with experimental data. The results of this comparison are reported in the next section. The experimental setup is a complex system which contains interaction between different parts of the system, particularly defective bearings. The analytical model developed in this work is a simple model to study the principle features of a defective bearing. This model does not take into account the interaction between two bearings.

6.2. Experimental validation

In this step of study, the simulation results of a defective rolling element bearing at the "drive end" containing single point defects on inner race, outer race and rolling elements are compared to experimental data. In order to reduce the effect of the noise on the gathered experimental data an orthogonal wavelet denoising was performed according to the procedure developed in Ref. [28]. After that, the frequency

Table 1
Dimensions of derive end bearing (deep-groove ball bearing type 6205-2RSL JEM SKF) in mm

Z	$2 \times R_i$	$2 \times R_o$	d	D
9	25	52	8	39

Table 2
Defect frequencies in Hz (for shaft speed 1750 rev/min ≈ 29.17 Hz)

ω_{bpi}	ω_{bpo}	ω_c	ω_b
157.94	104.56	11.62	68.74

Table 3
Size and depth of defects (in mil = 0.001 in)

	Inner race	Outer race	Rolling element
Size	7	7	7
Depth	7	7	7

Fig. 3. The test stand, picture by permission of Dr. Kenneth A. Loparo, Case Western Reverse Lab.

spectrum of the denoised signal can be produced using the conventional fast Fourier transform (FFT) to obtain frequency components in details.

Figs. 4a–d show the displacement and velocity response of a normal bearing without any defects. The response of the system reaches to steady state after a period of time. In Figs. 4e and f the original signal and the denoised signal are shown, respectively. The frequency spectrum of the denoised signal and those obtained from the velocity response of the proposed model are shown in Figs. 4g and h, respectively. As it can be seen in these two figures, corresponding spectrums included the expected frequency at the varying compliance frequency (104.56 Hz). The frequency spectrum of experimental data have a peak at 106 Hz and in the frequency response obtained from the proposed model, a peak occurs at 105.3 Hz. Since the results obtained from the experiment are all reported in mV it is not possible for authors to compare the response amplitude of the proposed model and experimental data. This frequency was detected both in horizontal and vertical frequency spectra of the velocity of the system but the amplitude of the horizontal spectrum are much higher than the vertical spectrum which is not clear in Fig. 4h. As a result, comparison of frequency content of analytical model and experimental test confirms the successful modeling of the effect in this analysis. There are also some other frequencies which are related to the operating frequency (1750 rev/min $\approx$ 29.17 Hz) of the system and the interaction between drive end and fan end bearings. The varying compliance frequency and ball passing outer race frequency of the fan end bearing are, respectively, 89.05 and 144.28 Hz. These frequencies are also appeared in the spectrum of experimental data which were not discussed in this analysis. But if we import the specification of this bearing in our model we can compute these frequency contents as well.

In Figs. 5a–d the displacement and velocity response for bearing with a single point defect on outer race are plotted. The size and depth of the defect are listed in Table 3. Although the response looks complex, it is still periodic. Fig. 5e shows the original signal obtained from an experiment on an outer race damaged bearing. Fig. 5f illustrates the gathered signal from the experimental test after denoising procedure. In Figs. 5g and h the frequency spectrum of the gathered signal and the simulated response are compared to each other. As it can be seen in these figures, the dominant frequency of the corresponding spectrums is the ball passing outer race frequency (104.56 Hz). It was explained in previous sections that even perfect bearings generates vibration at varying compliance frequency, ω_{vc} which is equal to ball passing outer race frequency. But in the presence of a local defect this frequency will be excited strongly which increases the amplitude of the vibration. The difference between a normal bearing without any defect and a defective one including local defects on outer race can be distinguished by comparing the vibration level of the response of the system at varying compliance frequency. From Figs. 4h and 5h it can be seen that the amplitude of the vibration (57 μm/s) at

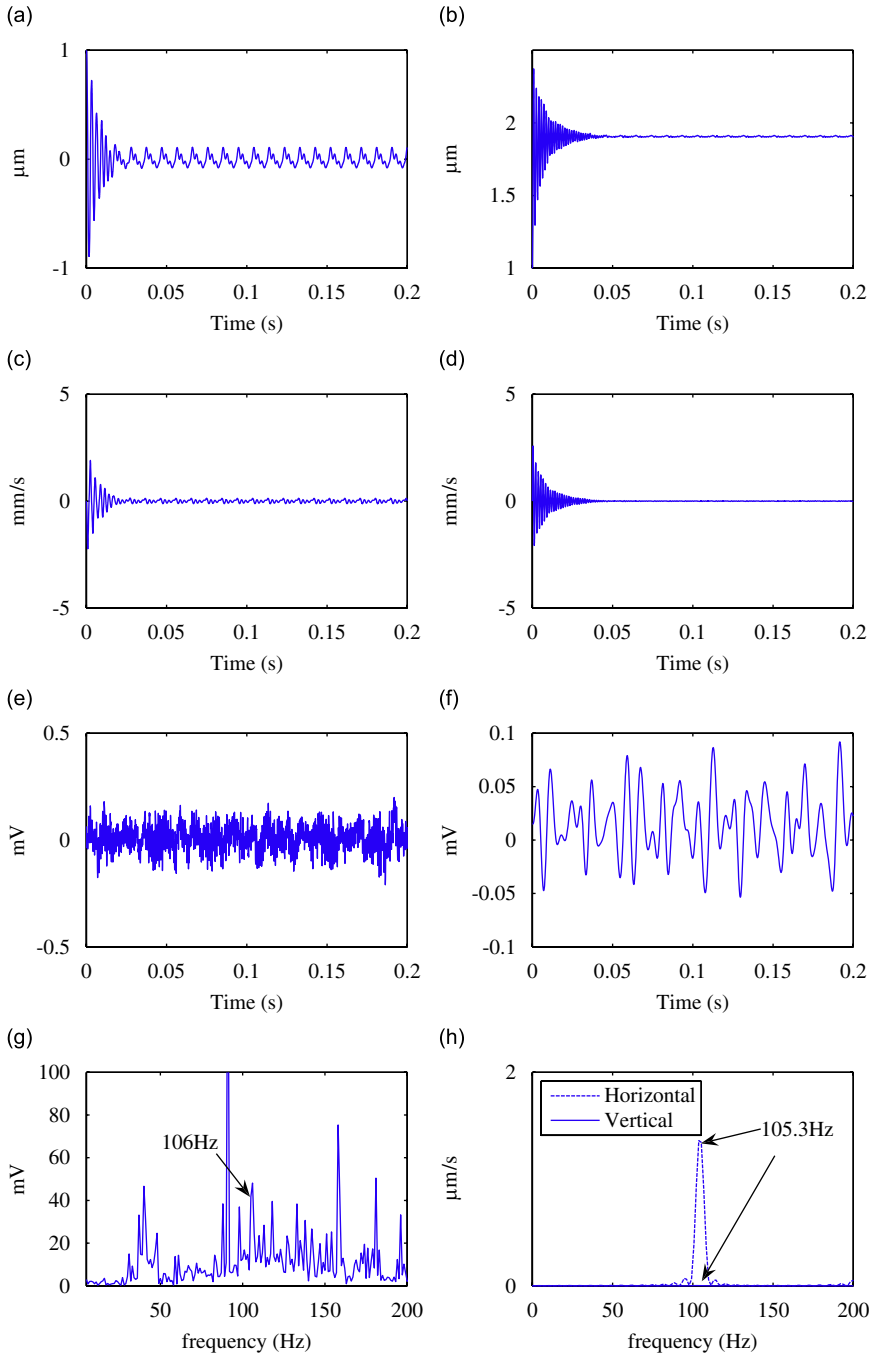

Fig. 4. Dynamic response of normal rolling element bearing: (a) horizontal displacement, (b) vertical displacement, (c) horizontal velocity, (d) vertical velocity, (e) experimental signal for normal bearing, (f) denoised signal for normal bearing, (g) experimental FFT for normal bearing and (h) FFT for normal bearing model.

this frequency (104.56 Hz) is considerably higher than the amplitude of the vibration for a normal bearing (1.36 μm/s).

For an inner race defect the displacement and velocity response of the system is shown in Figs. 6a–d. The same procedure is applied to the original signal gathered from experimental analysis and the denoised signal

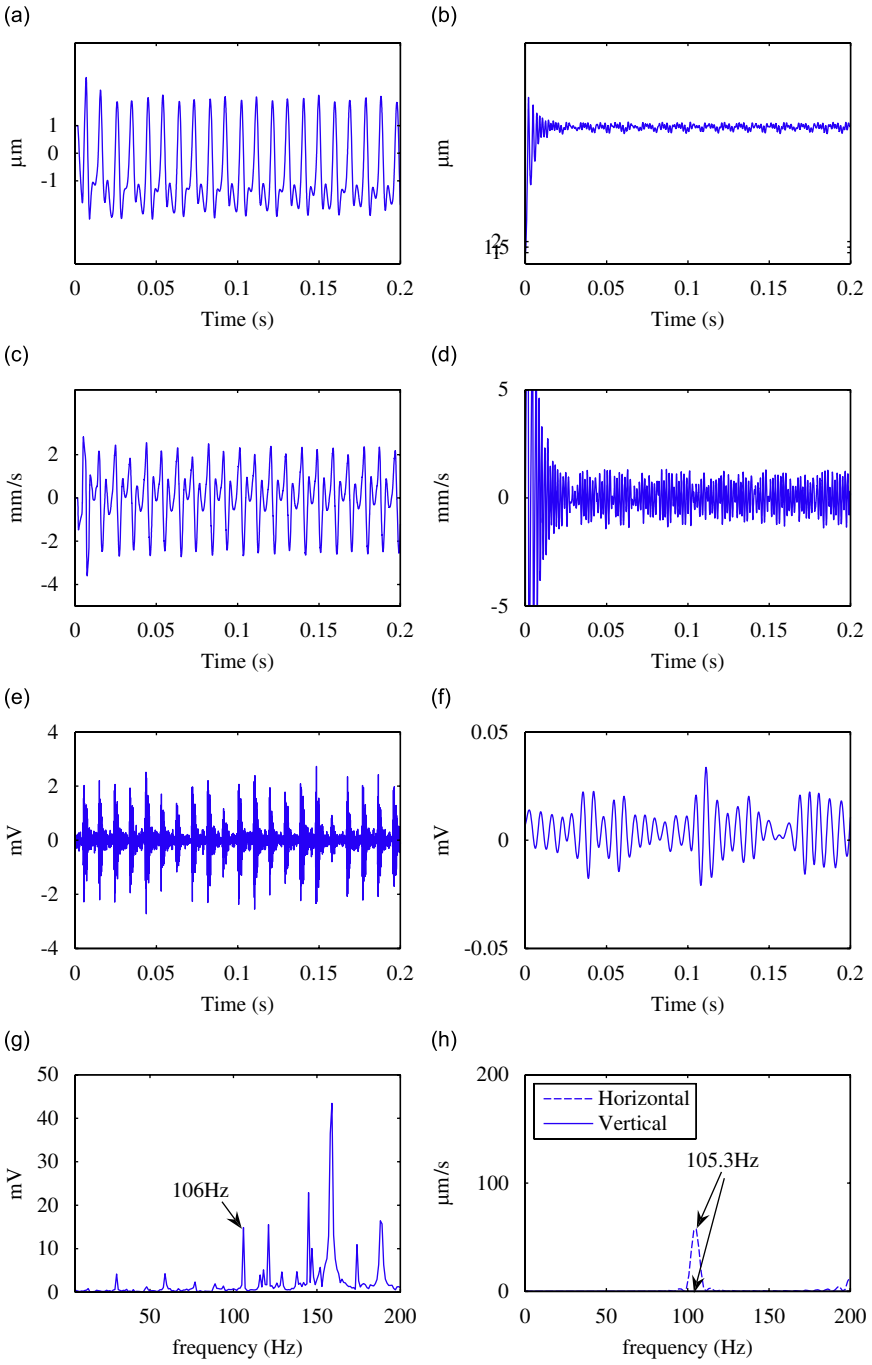

Fig. 5. Dynamic response of rolling element bearing with a single–point defect on its outer race: (a) horizontal displacement, (b) vertical displacement, (c) horizontal velocity, (d) vertical velocity, (e) experimental signal for outer race defect, (f) denoised signal for outer race defect, (g) experimental FFT for outer race defect and (h) FFT for outer race defect model.

which are shown in Fig. 6e and f, respectively. The fast Fourier transform of the denoised signal is shown in Fig. 6g. The frequency spectrum contains a dominant peak very close to ball passing inner race frequency (157.94 Hz). This figure shows a peak at 158 Hz. There is also a smaller peak around the varying compliance frequency (104.56 Hz). This peak is appeared in the frequency spectrum at 106 Hz. Fig. 6h is the frequency

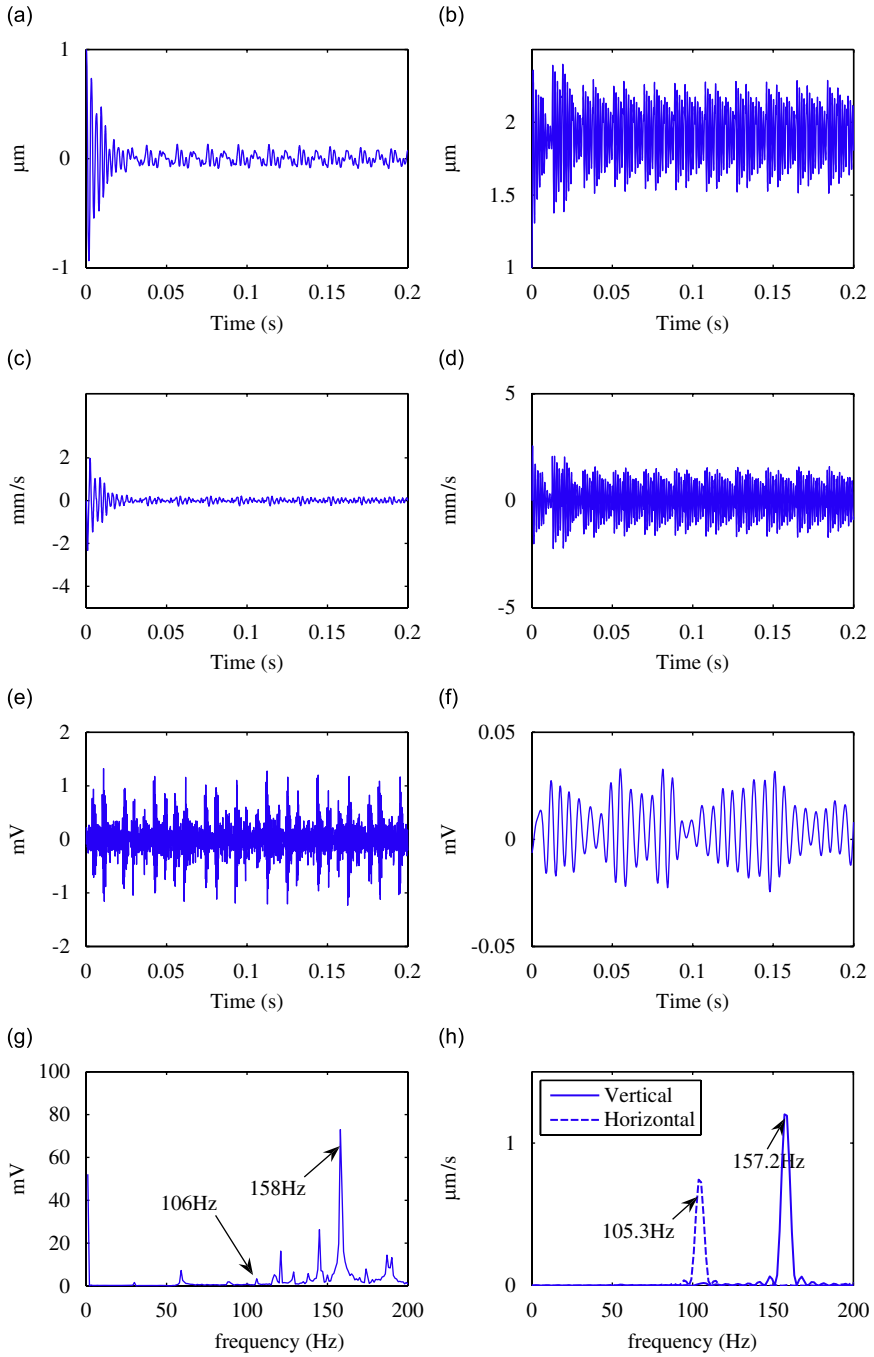

Fig. 6. Dynamic response of rolling element bearing with a single point defect on its inner race: (a) horizontal displacement, (b) vertical displacement, (c) horizontal velocity, (d) vertical velocity, (e) experimental signal for inner race defect, (f) denoised signal for inner race defect, (g) experimental FFT for inner race defect and (h) FFT for inner race defect model.

spectrum of the velocity response obtained from the proposed model. As it can be seen there is a dominant peak at 157.2 Hz which is almost near the ball passing inner race frequency.

At the end of this section, the effect of rolling element defect was studied. The displacement and velocity time response of the system are illustrated in Figs. 7a–d. The original and denoised signals corresponding to

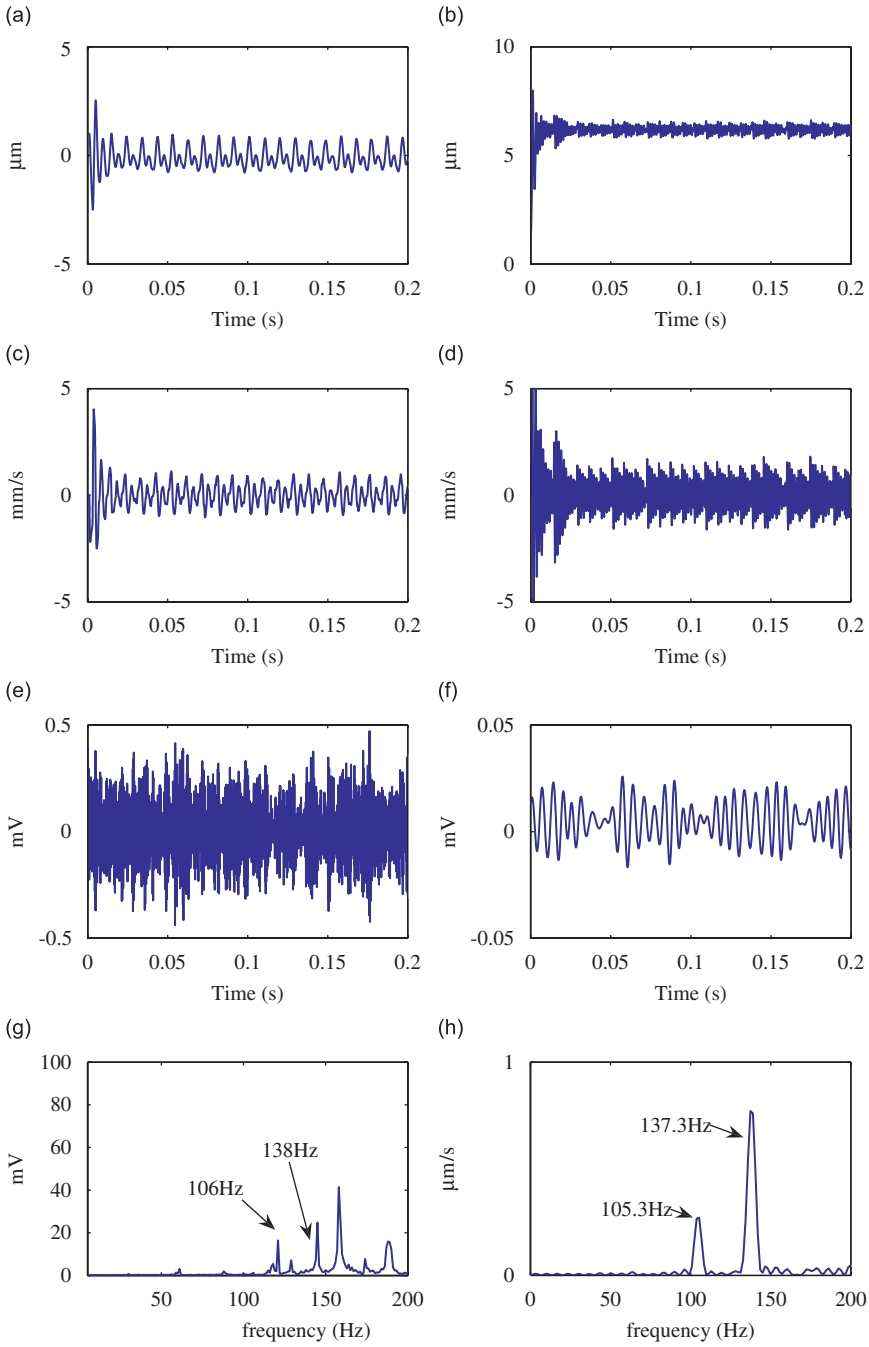

Fig. 7. Dynamic response of rolling element bearing with a single point defect on one of the rolling elements: (a) horizontal displacement, (b) vertical displacement, (c) horizontal velocity, (d) vertical velocity, (e) experimental signal for rolling element defect, (f) denoised signal for rolling element defect, (g) experimental FFT for rolling element defect and (h) FFT for rolling element defect model.

the bearing with a local defect on rolling elements are shown in Figs. 7e and f, respectively. The frequency spectra for the experimental and the simulated response of the system are compared to each other in Figs. 7g and h. In this case, there is a dominant peak around twice of ball spin frequency (137.48 Hz) in both spectra. This frequency was appeared in Fig. 7g at 138 Hz while in Fig. 7h it was appeared at 137.3 Hz. The varying compliance frequency is also appeared in the frequency spectrum of the system under investigation.

The above study shows that the main contributions of the frequency spectra obtained by the proposed model are in accordance with reported experimental spectra for various defect conditions.

6.3. Stability analysis

In this work, taking the shaft speed as a parameter of study, the effect of radial internal clearance in rolling element bearings contain local surface defects on raceways and rolling elements is studied. The dynamic model developed in this study used for investigation of instability and the route to chaos in the dynamic response of the system as the operating speed of the system is changed. The steady-state response of the rotor bearing system was obtained and the peak-to-peak response of the horizontal and vertical displacement plotted by numerical integration. The appearance of different regions of periodic, periodic doubling and chaotic behavior of the system for various local surface defects at different radial clearances would be discussed in this section.

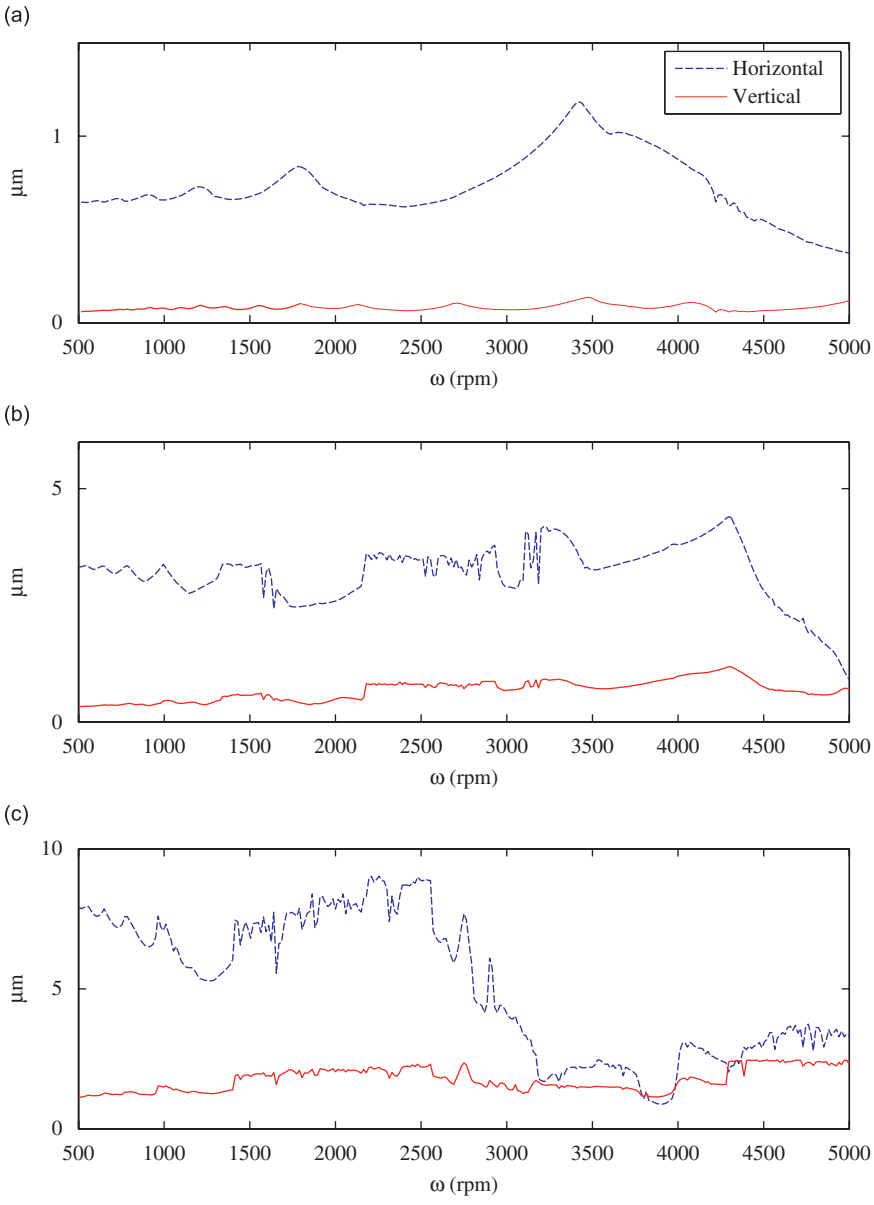

Fig. 8. Peak-to-peak displacement response of a normal bearing, (a) $\gamma = 5\,\mu m$, (b) $\gamma = 13\,\mu m$ and (c) $\gamma = 30\,\mu m$.

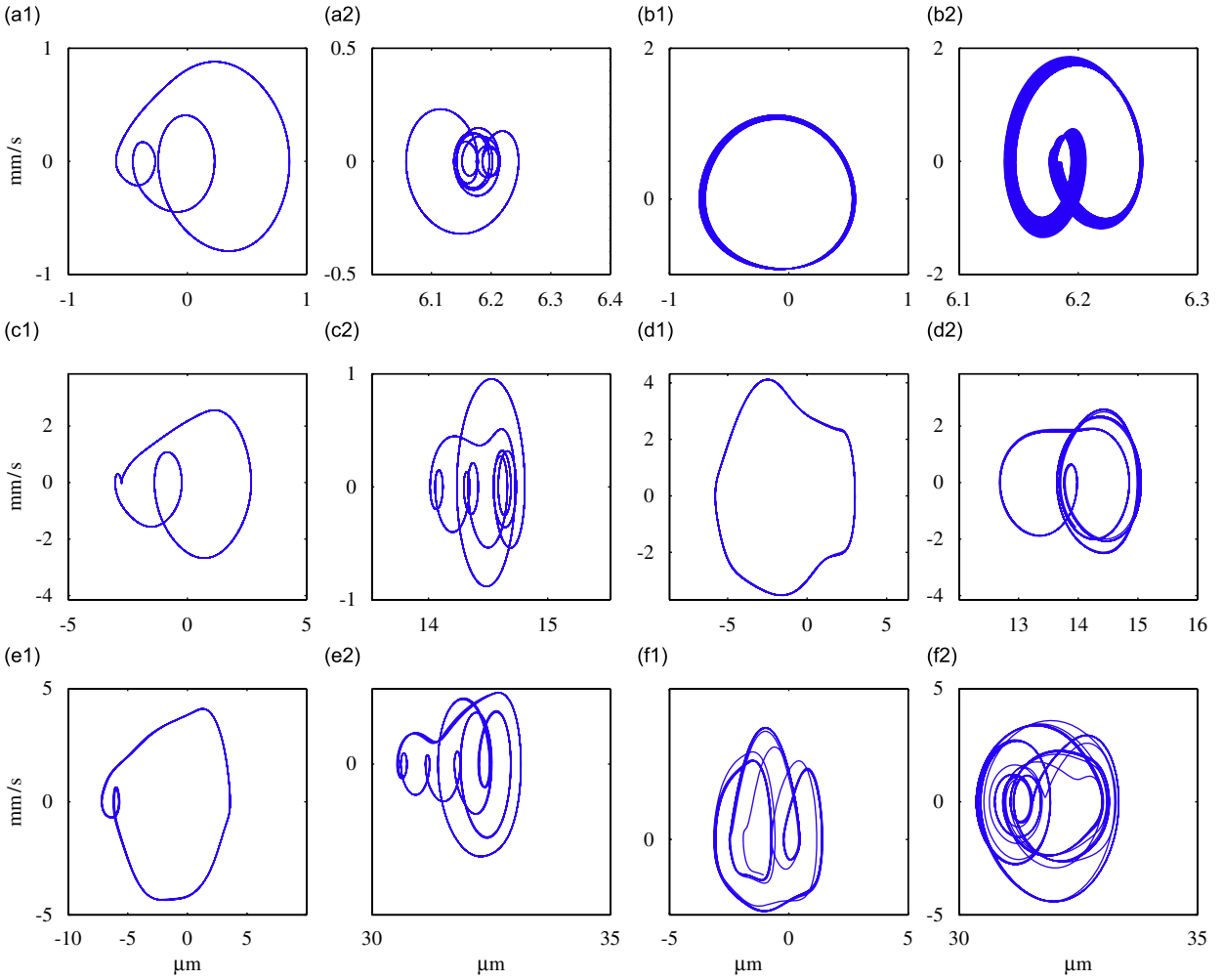

Fig. 9. The projection of phase trajectories for a normal bearing system, (a1,a2) $\omega = 1200$ rev/min, $\gamma = 5\,\mu$m, (b1,b2) $\omega = 4225$ rev/min, $\gamma = 5\,\mu$m (c1,c2) $\omega = 1200$ rev/min, $\gamma = 13\,\mu$m (d1,d2) $\omega = 4300$ rev/min, $\gamma = 13\,\mu$m, (e1,e2) $\omega = 1200$ rev/min, $\gamma = 30\,\mu$m, (f1,f2) $\omega = 3600$ rev/min, $\gamma = 30\,\mu$m, where 1 and 2 denotes horizontal and vertical vibration, respectively.

Fig. 8 shows the peak-to-peak displacement response of a bearing system without any defect in horizontal and vertical directions for three classes of radial internal clearance is shown for comparison. Fig. 9 illustrates the projection of phase trajectories for various radial clearances of a normal bearing rotor system. It can be seen from these figures that a continuous change in rotational speed of the shaft changes the shape of the chaotic motion.

Now, the peak-to-peak displacement response of a bearing system with single point defect on inner race, outer race and rolling elements would be studied. The peak-to-peak response and phase trajectories are plotted in horizontal and vertical directions for three classes of radial internal clearance. Considering the response over a large range of rotational speed, 500–5000 rev/min, the motion may be simply categorized at any particular speed to various regions.

Fig. 10a shows the response of a bearing system with single point defect on inner raceway with small radial clearance (5 μm). The response of the system indicates the characteristics of a softening nonlinear system. It contains peaks accompanied by jump phenomena and transition stages. The motion is completely chaotic at low speeds up to 1000 rev/min but as the speed increases the stability returns to the system and the transition stages grow off. In these regions, i.e. 1450–1600 or 2300–3200 rev/min, the motions is quasi-periodic because

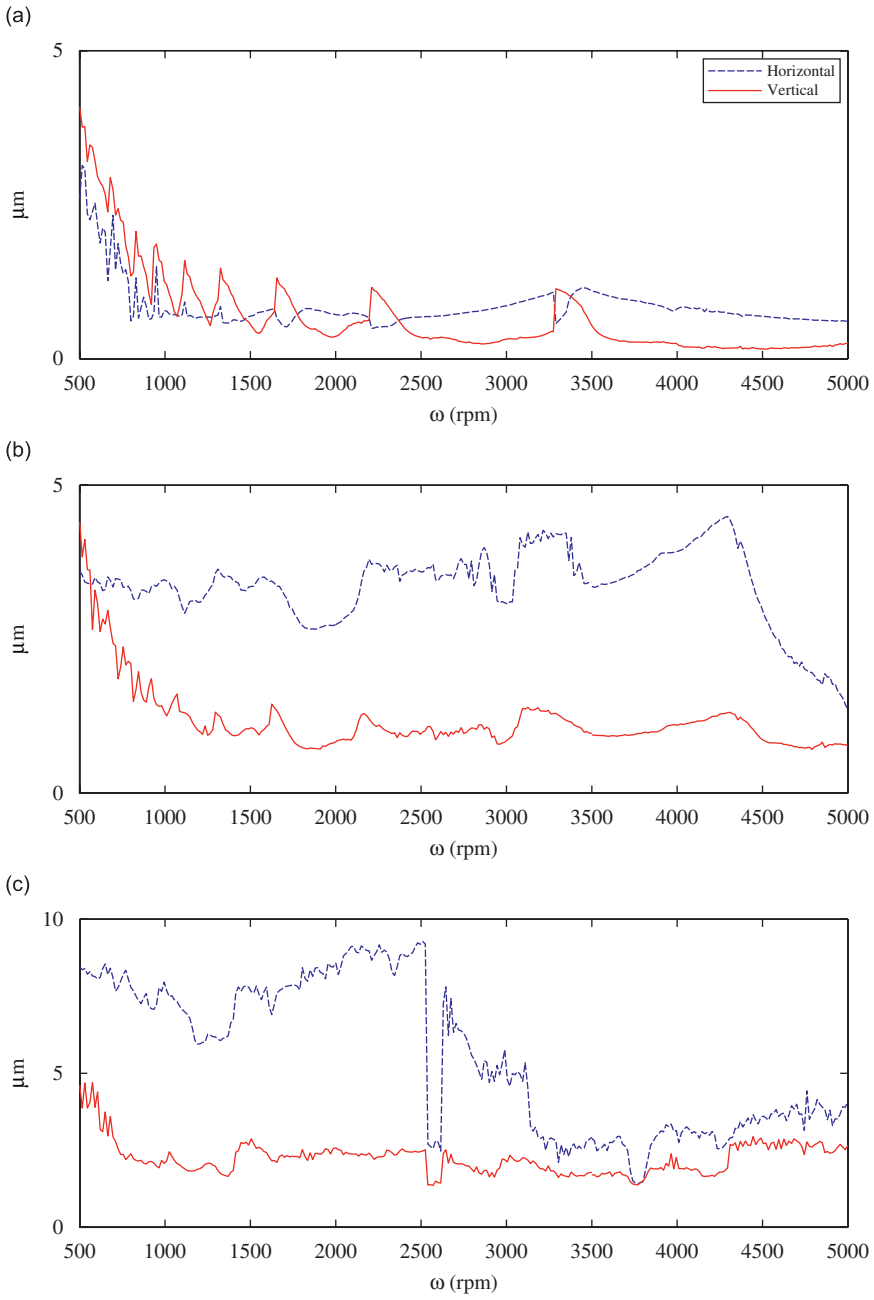

Fig. 10. Peak-to-peak displacement response of a bearing system with single point defect on inner raceway: (a) $\gamma = 5\,\mu m$, (b) $\gamma = 13\,\mu m$ and (c) $\gamma = 30\,\mu m$.

of the net structure of the phase trajectories and there are period doubling bifurcations. At the end of each stage, i.e. 1650 or 3290 rev/min, the fold bifurcation take places and the jump in the response of the system occurs. Because of this bifurcation, the motion leads to instability after which chaos suddenly appears. As speed increases the stability returns in next transition stage through period doubling bifurcations. At high shaft speeds the time responses show beating and chaotic behavior. The corresponding phase trajectories to the bearing with a single point fault on inner race and radial internal clearance of 5 μm is shown in Figs. 11a and b.

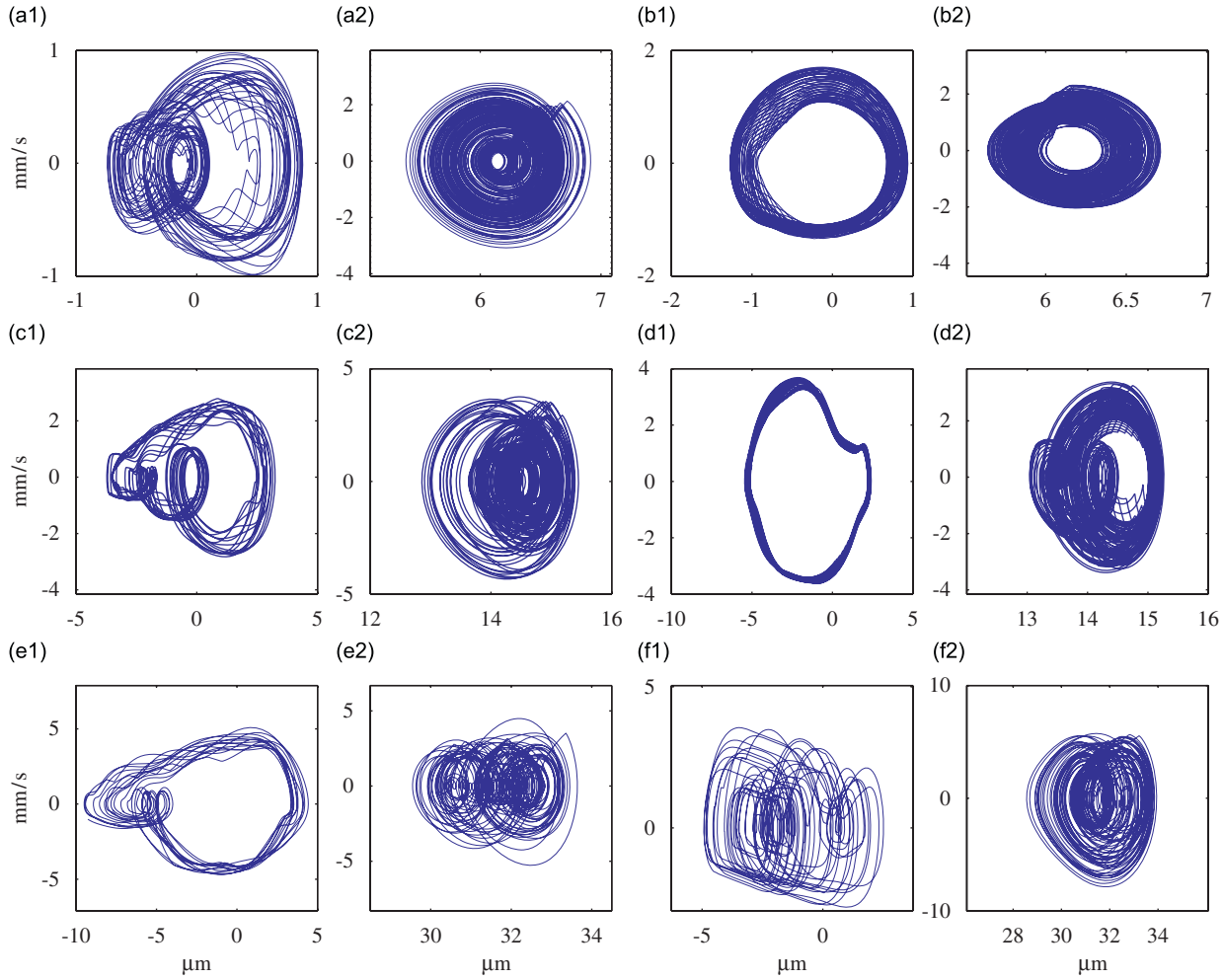

Fig. 11. The projection of phase trajectories for a bearing system with single point defect on inner raceway, (a1,a2) $\omega = 1640$ rev/min, $\gamma = 5\,\mu$m, (b1,b2) $\omega = 3500$ rev/min, $\gamma = 5\,\mu$m (c1,c2) $\omega = 1000$ rev/min, $\gamma = 13\,\mu$m (d1,d2) $\omega = 4000$ rev/min, $\gamma = 13\,\mu$m, (e1,e2) $\omega = 1100$ rev/min, $\gamma = 30\,\mu$m, (f1,f2) $\omega = 4700$ rev/min, $\gamma = 30\,\mu$m, where 1 and 2 denotes horizontal and vertical vibration, respectively.

The response of the system for radial clearance of 13 μm is shown in Fig. 10b. The phase trajectories for this case are plotted in Figs. 11c and d. Two regions of unstable response can be distinguished in this figure in which the chaotic motion may be preceded on one side by a cascade of period doubling bifurcations. At speed 1700 rev/min the stability returns to the system and up to 2100 rev/min the motion is quasi-periodic and there are period doubling bifurcations. As a dominant effect of increasing the radial clearance, the jump phenomena do not appear in the response as investigated for small clearances. The amplitude modulation in the frequency response indicates the system undergoing Hopf bifurcations, i.e. 2200 and 3100 rev/min, through which the quasi-periodic motion loses stability. In this case, the eigenvalues of the monodromy matrix leave the unit circle in the complex plane. The cascade of period doubling bifurcations gives way to chaotic solutions in these regions. As speed increases the chaotic response weakens to give way to quasi-periodic solutions. From 3000 to 5000 rev/min there are quasi-periodic responses which the stability of the system increases along the speed. The amplitude of the vibrations decreases after 4400 rev/min.

For a large radial clearance of 30 μm the response of a defective bearing containing a single point defect on its inner raceway is shown in Fig. 10c. The response pattern is quite different in comparison with two last cases. There are three speed ranges in which the periodic solution loses stability. The phase diagrams for a number of selected speeds are shown in Figs. 11e and f. The first speed range as depicted in Fig. 10c is from

500 up to 2500 rev/min. It has period doubling bifurcations. From speed 1400 up to 2000 rev/min the motion is quasi-periodic because of the net structure of phase trajectories. As speed increases up to 2500 rev/min the stability returns and the motion leads to periodic solutions. In the second speed range 2700–3700 rev/min the phase trajectories of the system have fractal structure which indicates the chaotic behavior of the system. After that, the stability returns and the motion becomes quasi-periodic. In the third region from 4000 to 5000 rev/min the quasi-periodic motion loses stability by the way of boundary crisis route to chaos.

In the case of an outer race defect, the response is shown in Fig. 12. Here also the stiffness softening characteristic of the system at small clearances is quite apparent. It can be seen from Fig. 12a that response

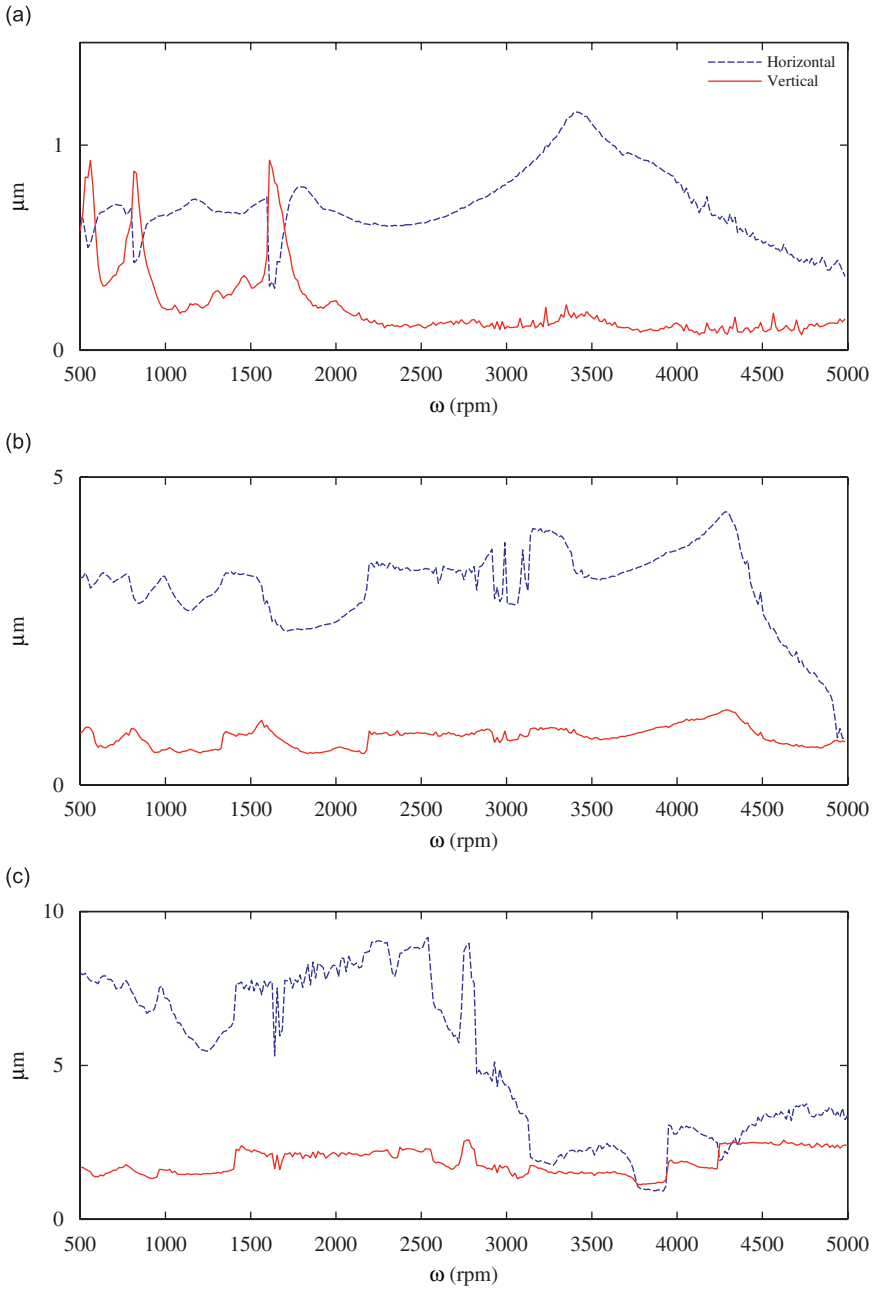

Fig. 12. Peak-to-peak displacement response of a bearing system with single point defect on outer raceway: (a) $\gamma = 5\,\mu m$, (b) $\gamma = 13\,\mu m$ and (c) $\gamma = 30\,\mu m$.

contains jump phenomena and transition stages. It was also observed that except around the jump regions the response curve is similar to those obtained from a normal bearing. The most important route to unstable periodic solutions along transition stages is period doubling. The jump phenomena occur through fold bifurcation in an interior crisis route to chaos. The sudden increase in the size of a chaotic attractor occurs while the chaotic attractor collides with periodic orbits in the interior of its basin. The interior crisis route to chaos induces intermittency in the system which leads to a permanent jump between two chaotic attractors. These are regions of multivalued solutions which it is difficult to find all periodic solutions by numerical integrations. The eigenvalues of the monodromy matrix cross from $+1$. Another pattern of transition response is periodic in waveform which occurs almost at high operational speeds which can be detected in Figs. 13a and b. The response for radial clearance of 13 μm is illustrated in Fig. 12b. Two regions can be identified which have unstable periodic motion. The response is almost similar to those obtained for inner race defect at this clearance. Here also two regions of unstable periodic response can be identified, i.e. from 500 to 1700 rev/min and also from 2100 to 3500 rev/min, but as depicted in Figs. 13c and d the orbits are fairly structured while for inner race defects the phase plot shows that more dense orbits points are surrounded by less dense points. Fig. 12c shows the response curve in the presence of outer race defect for large radial clearance $\gamma = 30$ μm. The response contains a region of high amplitude solution in the speed range of 500 up to 2600 rev/min. As the speed increase from 500 up to 1400 rev/min the stability of the system increases and there

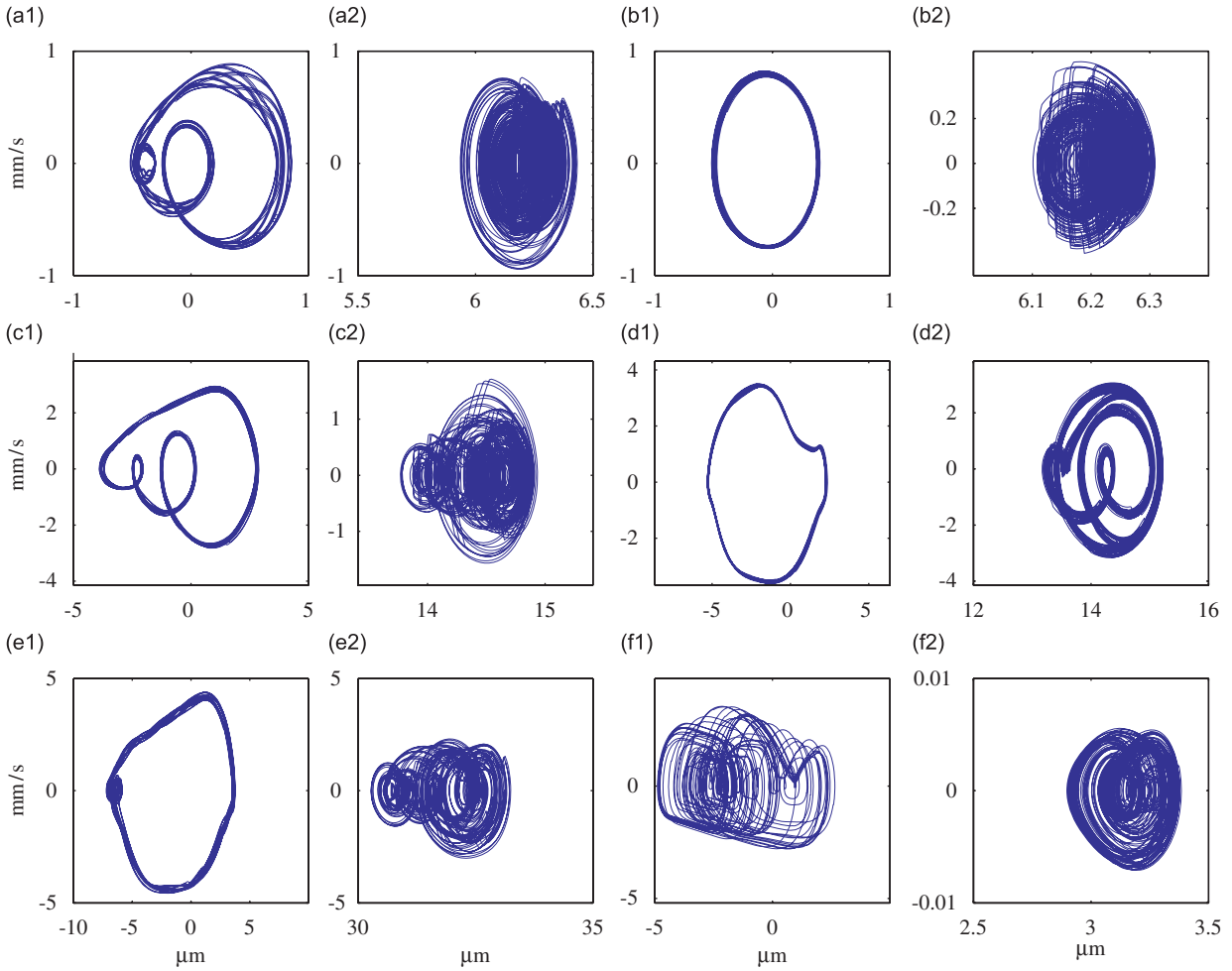

Fig. 13. The projection of phase trajectories for a bearing system with single point defect on outer raceway, (a1,a2) $\omega = 1265$ rev/min, $\gamma = 5$ μm, (b1,b2) $\omega = 4650$ rev/min, $\gamma = 5$ μm (c1,c2) $\omega = 1000$ rev/min, $\gamma = 13$ μm (d1,d2) $\omega = 4000$ rev/min, $\gamma = 13$ μm, (e1,e2) $\omega = 1250$ rev/min, $\gamma = 30$ μm, (f1,f2) $\omega = 4500$ rev/min, $\gamma = 30$ μm where 1 and 2 denotes horizontal and vertical vibration, respectively.

are period doubling bifurcations. From 1400 to 2500 rev/min the motion becomes quasi-periodic because of the net structure of phase trajectory. From 2600 to 3500 rev/min the chaos come out in a quasi-periodic route. The stability returns to the system in the range of 3800–3950 rev/min. As speed increases from 4000 rev/min, the collision of chaotic attractors with periodic orbits on their basin boundaries lead to sudden destruction of chaotic attractors and the boundary crisis route give way to chaos. The projection of phase trajectories for selected speeds is shown in Figs. 13e and f.

Now, the stability and the nature of the solution in presence of a single point defect on one of the rolling elements would be discussed. Fig. 14a shows the response curve for small value of radial clearance $\gamma = 5\,\mu m$.

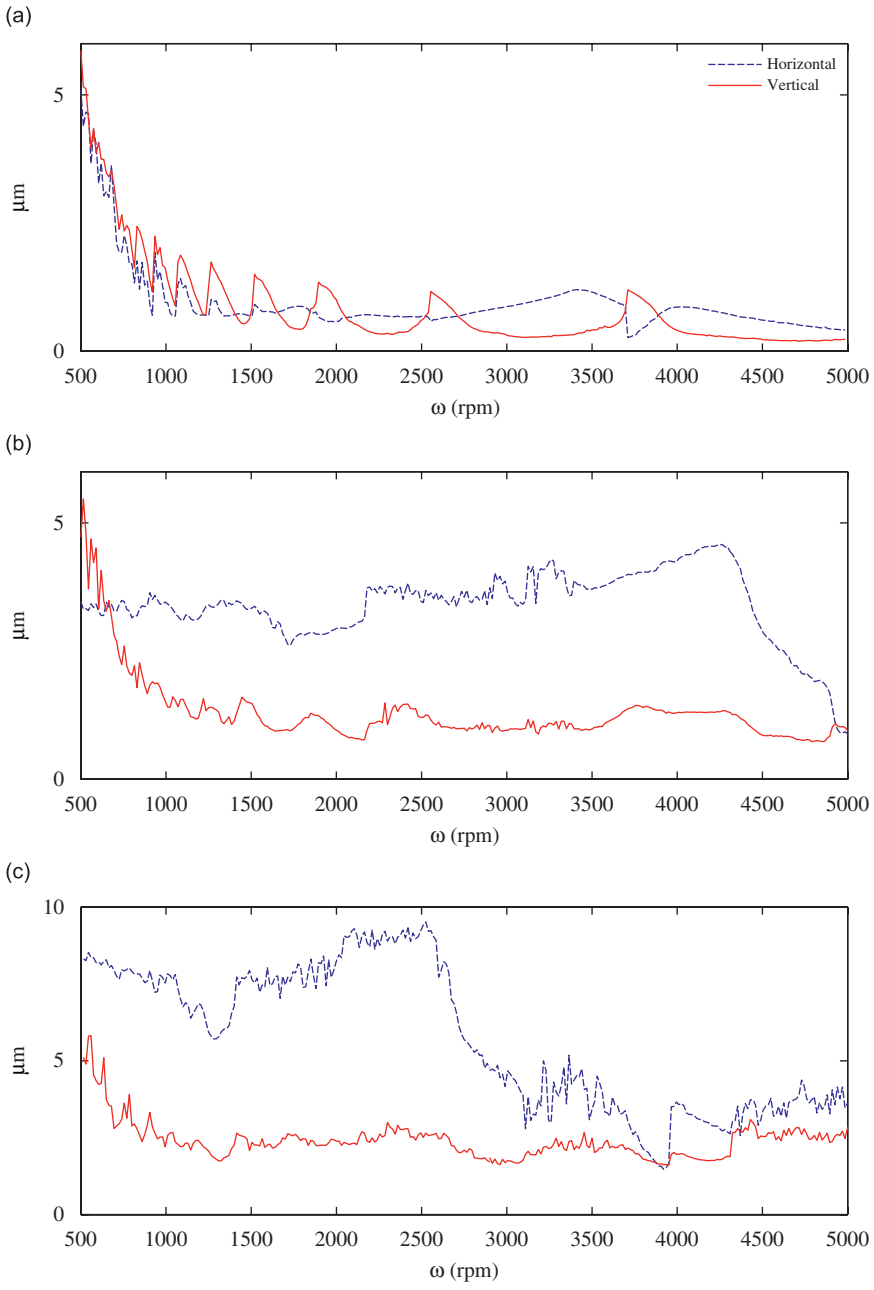

Fig. 14. Peak-to-peak displacement response of a bearing system with single point defect on rolling elements: (a) $\gamma = 5\,\mu m$, (b) $\gamma = 13\,\mu m$ and (c) $\gamma = 30\,\mu m$.

As it can be seen the response here also contains successive jump phenomena and transition stages. It can be seen that the response is similar to what was detected in the case of inner race defect at this clearance but the peaks in which jump occurs shifted to left in this figure. The basic route to chaos in small clearances is interior crisis. The nature of the motion in transition stages is quasi-periodic which is apparently can be identified from the projection of phase trajectories illustrated in Figs. 15a and b. In the regions far from jump peaks, the stability increases as speed increases. In Figs. 14b and c the peak-to-peak response is shown for radial internal clearances of 13 and 30 μm, respectively. As it can be seen from Fig. 14b there are two regions in which the motion is quasi-periodic and chaotic. Up to 1700 rev/min, the chaotic behavior in low speeds weakens through a period doubling route. In the speed range 1700–2000 rev/min the stability increases and the phase trajectories become fairly structured which indicates response reaches to periodic solution but it is not quite periodic. The second chaotic region starts at 2050 rev/min through Hopf bifurcation and the peak-to-peak response shows amplitude modulation. As speed increase up to 3000 rev/min the phase trajectory shows fractal structure which indicates chaotic motion. After that the stability returns to the system and the projection of phase trajectories change to net structure which is the representative of quasi-periodic solution. In Fig. 14c it was shown that for large clearance $\gamma = 30\,\mu m$, there are period doubling bifurcations up to 1700 rev/min. The region from 1700 to 2000 rev/min has unstable response due to Hopf bifurcations. It results in an amplitude modulation and quasi-periodic response. At 2050 rev/min the Hopf bifurcation occurs and

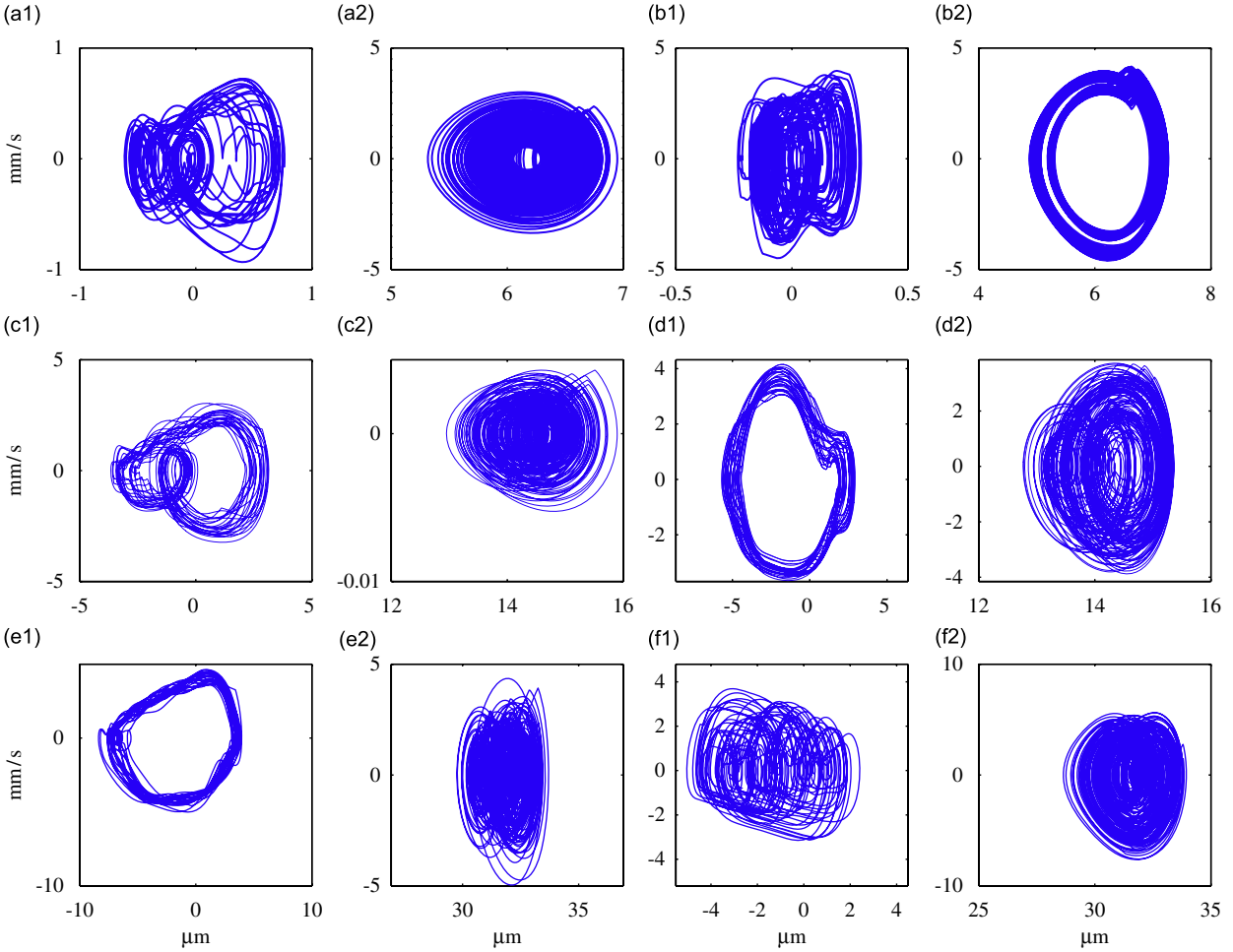

Fig. 15. The projection of phase trajectories for a bearing system with single point defect on rolling elements, (a1,a2) $\omega = 1500$ rev/min, $\gamma = 5\,\mu m$, (b1,b2) $\omega = 3710$ rev/min, $\gamma = 5\,\mu m$ (c1,c2) $\omega = 1250$ rev/min, $\gamma = 13\,\mu m$ (d1,d2) $\omega = 4000$ rev/min, $\gamma = 13\,\mu m$, (e1,e2) $\omega = 1295$ rev/min, $\gamma = 30\,\mu m$, (f1,f2) $\omega = 4900$ rev/min, $\gamma = 30\,\mu m$, where 1 and 2 denotes horizontal and vertical vibration, respectively.

again the peak-to-peak response goes up. The stability returns to the system at 2650 rev/min. As speed increases the chaotic response can be seen from 2900 to 3700 rev/min through a period doubling bifurcation route. The response changes to quasi-periodic from 3800 to 4200 rev/min. The chaotic response appears from 4200 rev/min. There are boundary crisis route to chaos in this region. The phase trajectories correspond to radial clearance $\gamma = 30\,\mu m$ are plotted in Figs. 15e and f.

7. Conclusion

In this paper the effect of local surface defects on the stability and the dynamic response of a rolling element bearing rotor system were investigated using an analytical model. The response of the bearing system was compared with those obtained from experiments. The accordance of the frequency components obtained from the mathematical model with those appeared in the frequency spectrum of the experimental data verifies the validity of the proposed model. It was investigated that the defect frequencies are slightly different from calculated values as a consequence of slipping and skidding in the rolling element bearings.

The linear stability analysis of the system indicates the existence of stable and unstable regimes in the response of the system. This analysis shows that in most range of shaft speeds, the system is not depended on initial conditions but strongly affected by the parameters of the system particularly radial internal clearance and surface defects. According to the results of the current simulation, the important routes to chaotic motion can be categorized as following:

For small radial clearance the basic route to chaos is interior crisis and jump phenomena though fold bifurcations. There are transition stages in which the period doubling is the usual route to instability and quasi-periodic solutions. The nonlinearity bends the frequency response to the left which indicates softening characteristic of the system. The bending of the frequency response leads to multivalued amplitudes and hence the jump phenomena. The location of defect at small clearance affects the frequency at which the jump occurs. For outer race defect the peaks occurs at low shaft speeds while in the case of inner race and rolling element defect the response contain several peaks as speed increases. The peak frequencies are different in each case.

For normal and large clearances the motion is quite unstable and in most speed ranges the system undergoing the quasi-periodic and chaotic motion. In this case the regions of unstable periodic motion would be extended. For normal clearances period doubling bifurcations and Hopf bifurcations are the usual routes to unstable periodic solutions while for large clearances the boundary routes to chaos also occurs especially at high speeds. The chaotic nature of motion rises up in the presence of rolling element defects while the outer race defect has minimal effect on unstable routes to chaos. It can be observed especially at high-speed ranges.

The current study gives designers a powerful tool for prediction of the trends of instability in rolling element bearing rotor systems in the presence of local surface defects. The proposed model can be used for design, predictive maintenance and also condition monitoring of machines.

Acknowledgment

The authors would like to thank Dr. Kenneth A. Loparo for his excellent technical help for the experimental aspects of the work.

Appendix A

For a bearing with a stationary outer race, the defect frequencies are given by the following expressions [23]:
The rotational speed of the cage

$$\omega_c = \frac{\omega}{2}\left(1 - \frac{d}{D}\cos\alpha\right) \tag{A.1}$$

The outer race defect frequency

$$\omega_{bpo} = Z\omega_c = \frac{Z\omega}{2}\left(1 - \frac{d}{D}\cos\alpha\right) \tag{A.2}$$

The inner race defect frequency

$$\omega_{\mathrm{bpi}} = Z(\omega - \omega_c) = \frac{Z\omega}{2}\left(1 + \frac{d}{D}\cos\alpha\right) \tag{A.3}$$

The ball spinning frequency

$$\omega_b = \frac{\omega}{2}\left(\frac{D}{d} - \frac{d}{D}\cos^2\alpha\right) \tag{A.4}$$

Appendix B

According to Hertzian theory, the geometry of a point contact is described by four radii of curvature. By definition, convex surfaces have positive radii and concave surfaces have negative radii. For a rolling element bearings are defined as

For inner race contact

$$R_{1x} = r, \quad R_{1y} = r, \quad R_{2x} = \frac{R}{\cos\alpha} - r, \quad R_{2y} = -R_i \tag{B.1}$$

And for outer race contact

$$R_{1x} = r, \quad R_{1y} = r, \quad R_{2x} = -\left(\frac{R}{\cos\alpha} + r\right), \quad R_{2y} = -R_o \tag{B.2}$$

The reduced radius of curvature R_{red} is defined as

$$\frac{1}{R_{\mathrm{red}}} = \frac{1}{R_x} + \frac{1}{R_y} \tag{B.3}$$

where

$$\frac{1}{R_x} = \frac{1}{R_{1x}} + \frac{1}{R_{2x}}, \qquad \frac{1}{R_y} = \frac{1}{R_{1y}} + \frac{1}{R_{2y}} \tag{B.4}$$

The equivalent modulus of elasticity is defined by the following relation:

$$\frac{2}{E_{\mathrm{eq}}} = \frac{1 - v_1^2}{E_1} + \frac{1 - v_2^2}{E_2} \tag{B.5}$$

In which E_1 and E_2 are the modulus of elasticity of the inner and the outer race and v_1 and v_2 are the Poisson's ratio, respectively. In the case of a dry point contact, the nonlinear contact stiffness is obtained from the Hertzian solution

$$K = \frac{\pi e E_{\mathrm{eq}}}{3k}\sqrt{\frac{2\varepsilon R_{\mathrm{red}}}{k}} \tag{B.6}$$

where k and ε denote the first and second kind of elliptic integral and e is the ellipticity parameter. To avoid numerical integration the following approximation formula used in calculations:

$$k = 1.5277 + 0.6203\ln\left(\frac{R_y}{R_x}\right) \tag{B.7}$$

$$\varepsilon = 1.0003 + 0.5968\left(\frac{R_x}{R_y}\right) \tag{B.8}$$

$$e = 1.0339\left(\frac{R_y}{R_x}\right)^{0.6360} \tag{B.9}$$

Appendix C

The elements of matrix **A** can be calculated as

$$\mathbf{A} = \begin{bmatrix} 0 & 0 & 1 & 0 \\ 0 & 0 & 0 & 1 \\ A_{xx} & A_{xy} & -c/m & 0 \\ A_{yx} & A_{yy} & 0 & -c/m \end{bmatrix} \tag{C.1}$$

where

$$A_{xx} = -\frac{1}{m}\frac{\partial f_x}{\partial x} = -\frac{3K}{2m}\sum_{j=1}^{Z}\gamma_j\delta_j^{1/2}\cos^2\theta_j \tag{C.2}$$

$$A_{xy} = A_{yx} = -\frac{1}{m}\frac{\partial f_x}{\partial y} = -\frac{1}{m}\frac{\partial f_y}{\partial x} = -\frac{3K}{2m}\sum_{j=1}^{Z}\gamma_j\delta_j^{1/2}\cos\theta_j\sin\theta_j \tag{C.3}$$

$$A_{yy} = -\frac{1}{m}\frac{\partial f_y}{\partial y} = -\frac{3K}{2m}\sum_{j=1}^{Z}\gamma_j\delta_j^{1/2}\sin^2\theta_j \tag{C.4}$$

References

[1] C.S. Sunnersjo, Varying compliance vibrations of rolling bearings, *Journal of Sound and Vibration* 58 (3) (1978) 363–373.
[2] T.E. Tallian, O.G. Gustafsson, Progress in rolling bearing vibration research and control, *ASLE Transactions* 8 (3) (1965) 195–207.
[3] C.S. Sunnersjo, Rolling bearing vibrations—geometrical imperfections and wear, *Journal of Sound and Vibration* 98 (4) (1985) 455–474.
[4] N. Tandon, A. Choudhury, A review of vibration and acoustic measurement methods for the detection of defects in rolling element bearings, *Tribology International* 32 (1999) 469–480.
[5] H. Ocak, K.A. Loparo, Estimation of the running speed and bearing defect frequencies of an induction motor from vibration data, *Mechanical Systems and Signal Processing* 18 (2004) 515–533.
[6] L.B. Jack, A.K. Nandi, Support vector machines for detection and characterization of rolling element bearing faults, *Proceedings of the Institution of Mechanical Engineers C—Journal of Mechanical Engineering Science* 215 (2001) 1065–1074.
[7] V. Purushotham, S. Narayanan, S.A.N. Prasad, Multi-fault diagnosis of rolling bearing elements using wavelet analysis and hidden Markov model based fault recognition, *NDT&E International* 38 (8) (2005) 654–664.
[8] F.P. Wardle, Vibration forces produced by waviness of the rolling surfaces of thrust loaded ball bearings—part 1: theory, *Proceedings of the Institution of Mechanical Engineers C—Journal of Mechanical Engineering Science* 202 (C5) (1988) 305–312.
[9] N. Aktürk, The effect of waviness on vibrations associated with ball bearings, *Transactions of the ASME—Journal of Tribology* 121 (1999) 667–677.
[10] N. Lynagh, H. Rahnejat, M. Ebrahimi, R. Aini, Bearing induced vibration in precision high speed spindles, *International Journal of Machine Tool Design and Research* 40 (2000) 561–577.
[11] S.P. Harsha, K. Sandeep, R. Prakash, Nonlinear dynamic behaviors of rolling element bearings due to surface waviness, *Journal of Sound and Vibration* 272 (3–5) (2004) 557–580.
[12] P.D. McFadden, J.D. Smith, Model for the vibration produced by a single point defect in a rolling element bearing, *Journal of Sound and Vibration* 96 (1) (1984) 69–82.
[13] P.D. McFadden, J.D. Smith, The vibration produced by multiple point defect in a rolling element bearing, *Journal of Sound and Vibration* 98 (2) (1985) 263–273.
[14] T. Zoladz, E. Earhart, T. Fiorucci, Bearing defect signature analysis using advanced nonlinear signal analysis in a controlled environment, NASA Technical Memorandum, 1995, 108491.
[15] N. Tandon, A. Choudhury, An analytical model for the prediction of the vibration response of rolling element bearings due to a localized defect, *Journal of Sound and Vibration* 205 (3) (1997) 275–292.
[16] J. Sopanen, A. Mikola, Dynamic model of a deep-groove ball bearing including localized and distributed defects—part 1: theory, *Proceedings of the Institution of Mechanical Engineers K—Journal of Multi-body Dynamics* 217 (2003) 201–211.

[17] J. Sopanen, A. Mikola, Dynamic model of a deep-groove ball bearing including localized and distributed defects—part 2: implementation and results, *Proceedings of the Institution of Mechanical Engineers K—Journal Multi-body Dynamics* 217 (2003) 213–223.
[18] M. Cao, A. Xiao, A comprehensive dynamic model of double-row spherical roller bearing—model development and case studies on surface defects, preloads, and radial clearance, *Mechanical Systems and Signal Processing* 22 (2007) 467–489.
[19] M. Tiwari, K. Gupta, O. Prakash, Effect of radial internal clearance of a ball bearing on the dynamics of a balanced horizontal rotor, *Journal of Sound and Vibration* 238 (5) (2000) 723–756.
[20] S.P. Harsha, Nonlinear dynamic analysis of an unbalanced rotor supported by roller bearing, *Chaos, Solitons & Fractals* 26 (2005) 47–66.
[21] S. Fukata, E.H. Gad, T. Kondou, T. Ayabe, H. Tamura, On the radial vibrations of ball bearings (computer simulation), *Bulletin of the JSME* 28 (1985) 899–904.
[22] K.J. Bathe, *Finite Element Procedures in Engineering Analysis*, Prentice-Hall, Englewood Cliffs, NJ, 1982.
[23] T.A. Harris, M.N. Kotzalas, *Essential Concepts of Bearing Technology, Rolling Bearing Analysis*, fifth ed., Wiley, New York, 2007.
[24] H. Prashad, *Solving Tribology Problems in Rotating Machines*, Woodhead Publishing, England, 2006.
[25] J. Courrech, R.L. Eshleman, in: C.M. Harris (Ed.), *Condition Monitoring of Machinery, Harris' Shock and Vibration Handbook*, fifth ed., McGraw-Hill, New York, 2002.
[26] T. Kapitaniak, S.R. Bishop, *The Illustrated Dictionary of Nonlinear Dynamics and Chaos*, Wiley, New York, 1999.
[27] V.S. Anishchenko, V. Astakhov, A. Neiman, T. Vadivasova, L. Schimansky-Geier, *Nonlinear Dynamics of Chaotic and Stochastic Systems*, Springer, Berlin, 2007.
[28] S. Abbasion, A. Rafsanjani, A. Farshidianfar, N. Irani, Rolling element bearings multi-fault classification based on the wavelet denoising and support vector machine, *Mechanical Systems and Signal Processing* 21 (2007) 2933–2945.